Earth and Planetary Science Letters 564 (2021) 116881

Contents lists available at ScienceDirect

Earth and Planetary Science Letters

www.elsevier.com/locate/epsl

Black Sea paleosalinity evolution since the last deglaciation reconstructed from alkenone-inferred Isochrysidales diversity

Yongsong Huang [a,*], Yinsui Zheng [a,b], Patrick Heng [a], Liviu Giosan [c], Marco J.L. Coolen [d]

[a] Department of Earth, Environmental and Planetary Science, Brown University, Providence, RI 02912, USA
[b] Ecosystems Center, Marine Biological Laboratory, Woods Hole, MA 02543, USA
[c] Geology and Geophysics, Woods Hole Oceanography Institution, Woods Hole, MA 02543, USA
[d] Curtin University, School of Earth and Planetary Sciences, WA Organic and Isotope Geochemistry Centre (WA-OIGC), Bentley, WA 6102, Australia

ARTICLE INFO

Article history:
Received 9 May 2020
Received in revised form 26 February 2021
Accepted 6 March 2021
Available online 31 March 2021
Editor: Y. Asmerom

Keywords:
Black Sea
alkenones
salinity
Isochrysidales
RIK_{37}
group I

ABSTRACT

The Black Sea underwent dramatic changes in salinity from the last glacial maximum to Holocene as it evolved from a large inland lake to become a part of the global ocean due to post-glacial sea level rise. However, the detailed history of the re-connection of the Black Sea to the Mediterranean and the resulting Black Sea salinity variations have been heavily debated. We take advantage of our recent study on alkenones from phylogenetically classified haptophyte groups and their association with variable salinity levels in modern environments to reconstruct detailed salinity changes in the Black Sea over the past 16,000 years. We report the first discovery and documentation of alkenones from Group I Isochrysidales in relation to past salinity changes in the Unit III sediment. Our data indicate that the Black Sea surface salinity gradually increased from near fresh at ~16 ka (~1-2 psu) to oligohaline (~ 5-6 psu) at ~ 9.4 ka, the time of initial marine inflow, suggesting a negative regional hydrological balance. Although the IMI (initial marine inflow) occurred at 9.4 ka, the relatively low surface water salinity levels persisted to the beginning of sapropel formation at 7.6 ka, suggesting a strongly positive regional hydrological balance. Alkenone profiles also indicate a period of significantly reduced salinity between 3.5 and 1.6 ka, differing from the previous proposed peak salinity at 2.7 ka based on alkenone hydrogen isotope values. We demonstrate that the mismatch originates from the predominance of previously unidentified Group II Isochrysidales over *E. huxleyi* during this time interval, and when species-specific hydrogen isotopic fractionation of alkenones is taken into consideration, the isotope-inferred salinity between 3.5 and 1.6 ka is consistent with our proposal. Our new assessment of the Black Sea salinity evolution since the last glacial shows broad agreement with other regional records and provides a new basis for evaluating the impact of regional hydrological changes on Neolithic human migrations to Europe.

1. Introduction

The Black Sea contains a rich sedimentary archive for studying the paleo-environmental history of the eastern Mediterranean, one of the key centers of the agriculture revolution and civilization in the world (Giosan et al., 2012; Turney and Brown, 2007). The successional changes in the environments of the Black Sea have been proposed to be the key trigger of the Neolithic culture transition in Europe (Ryan and Pitman, 1998; Turney and Brown, 2007). There are three litho-stratigraphic units (Unit I, Unit II and Unit III) of the Black Sea sediment during the late Quaternary (Ross and Degens, 1974), corresponding to major phases of its environmental evolution. Before the reconnection to the Mediterranean, the Black Sea is indicated to have existed as a fresh to brackish lake (Ross and Degens, 1974; Yanchilina et al., 2017). Due to the post-glacial sea level rise, the Black Sea Lake was reconnected with Mediterranean when the Bosporus sill was breached between 7,000 and 10,000 years ago (Aksu et al., 2002; Ballard et al., 2000; Herrle et al., 2018; Major et al., 2006; Ross and Degens, 1974; Soulet et al., 2011; Yanchilina et al., 2017; Ankindinova et al., 2019). Disagreements related to the proposed timing of reconnection of the Black Sea and the Mediterranean are primarily due to uncertainties in dating and reservoir ages, although more recent literature puts the reconnection (the initial marine inflow, IMI) at around 9.4 - 9 ka (Major et al., 2006; Coolen et al., 2013; Soulet et al., 2011; Yanchilina et al., 2017). A sapropel layer, known as Unit II, started deposition at around 7.6 ka. This Unit deposited for ~4,800 years ending at ~ 2.7 ka. A transitional sapropel layer deposited between 2.7 and 1.6 ka separates the first and last invasions of

* Corresponding author.
E-mail address: Yongsong_Huang@brown.edu (Y. Huang).

https://doi.org/10.1016/j.epsl.2021.116881
0012-821X/

Emiliania huxleyi, with the last invasion marked by the microlaminated coccolithophore ooze (Hay et al., 1991; Jones and Gagnon, 1994; Ross and Degens, 1974). The boundary between Unit I and Unit II was set at 2.7 ka by Hay et al. (1991), or at 1.6 ka by Ross and Degens (1974).

There remain major disputes concerning the salinity history of the Black Sea. For example, a cataclysmic flood event has been proposed to have resulted from the marine reconnection between the Black Sea and the open ocean, with the water level of the Black Sea rising abruptly for more than 100 meters within a few years (Ryan et al., 1997) or a few decades (Yanchilina et al., 2017). This hypothesis gained significant popular press as it was suggested to have inspired the biblical flood legend (Ryan and Pitman, 1998). However, other studies have proposed a more gradual reconnection to the ocean between 9.4 and 7.5 ka (Major et al., 2006; Yanko-Hombach et al., 2007; Coolen et al., 2013; Giosan et al., 2012). The key disagreement arises from different proxies used for reconstructing the water level of the Black Sea and, to a lesser extent, age model uncertainties (Aksu et al., 2002; Giosan et al., 2012; Hiscott et al., 2007; Hiscott and Aksu, 2002; Konikov et al., 2007; Yanchilina et al., 2017). Salinization of the Black Sea Lake was proposed to be gradual rather than abrupt according to micropaleontological and ancient sedimentary DNA (*sed* aDNA) reconstructions (Aksu et al., 2002; Coolen et al., 2013; Mertens et al., 2009; Soulet et al., 2011, 2010).

Based on $\delta^{18}O$ values of the foraminifera *Turborotalita quinqueloba*, Aksu et al. (2002) estimated the salinity of the Black Sea Lake to be 16 - 17 psu in Unit III. Similarly, the record of the dinoflagellate cyst *Lingulodinium machaerophorum* suggests that the Black Sea salinity ranged from 12 to 15 psu during the Unit III deposition, and 14 to 17 psu during the past 10,000 years (Mertens et al., 2012). However, these proposals contradict the freshwater biota fossils found in the Black Sea Unit III deposition period (e.g., Filipova-Marinova et al., 2013; Marret et al., 2009; Yanchilina et al., 2017), as well as ostracode-inferred salinity of 5 to 8 psu in the Unit III (Briceag et al., 2019). High salinity in Unit III was also contradicted by *sed* aDNA data, which revealed a predominance of freshwater plankton and fauna in Unit III sediments between 11.4 and 9.4 ka BP, mixed with a small percentage of DNA from typically marine plankton (Coolen et al., 2013). Moreover, salinity reconstruction using hydrogen isotopic (δD) values of long chain alkenones (LCA) suggests a peak salinity of $\sim$ 30 psu at 2.7 ka (Coolen et al., 2013; Giosan et al., 2012; van der Meer et al., 2008). This δD-reconstructed salinity peak was 10 psu higher than the salinity estimated by Aksu et al. (2002) and Mertens et al. (2012). One caveat of the alkenone δD estimate is that the reconstruction assumed that alkenones were predominantly produced by *Emiliania huxleyi* during the past 5200 years (Coolen et al., 2013). The latter study used a targeted *sed* aDNA approach to reconstruct the calcified as well as non-calcified haptophyte composition in the Black Sea since the onset of sapropel deposition $\sim$7.5 ka BP but may have failed to identify the full range of possible alkenone producers, notably the brackish Group II Isochrysidales.

Systematic analysis of haptophyte culture samples has revealed major molecular features that allow quantitative or semi-quantitative assessment of changes in the Isochrysidales species in environmental samples (Zheng et al., 2019). New analytical methods for the detection and separation of alkenones were applied to sediments from Black Sea core GGC18 (*sed* aDNA results from this core published by Coolen et al., 2009, 2013). We use the Baltic Sea surface sediment study by Kaiser et al. (2019) as the framework for interpreting Black Sea salinity changes over the last 16 kyr. The Baltic Sea is characterized by a large horizontal pelagic salinity gradient (0 to 35 psu) over 2000 km, encompassing the full habitat salinity ranges of Group I, II and III Isochrysidales (Theroux et al., 2010; Longo et al., 2016; Weiss G. et al., 2020). Changes in alkenone distributions along the modern Baltic Sea salinity gradient are primarily dictated by sea surface salinity and can be used to infer past salinity changes in the Black Sea since the last glacial.

2. Materials and methods

2.1. Samples

Sediments for this study were taken from the Giant Gravity Core GGC18 collected from the western basin of the Black Sea (42°46.569″N; 28°40.647″E; Fig. S1) in September 2006. This core was recovered from a water depth of 971 m during cruise AK06 on the R/V *Akademik* (Fig. S1, Coolen et al., 2009).

We use the Unit division points as defined in Hay et al. (1991). The total length of the sediment core is 337 cm, spanning Unit I (0 – 48 cm), Unit II (48 - 123 cm) and Unit III (123 - 337 cm) of the Black Sea. We subsampled 1 cm slices ($\sim$ 3 cc) from every other 1 cm-interval for the present study. A total of 167 samples were collected, including 24 samples from Unit I, 37 samples from Unit II and 106 samples from Unit III.

2.2. Age model

A few studies have been conducted previously to investigate the Unit I and II sections of GGC18 (Coolen, 2011; Coolen et al., 2013, 2009; Filipova-Marinova et al., 2013; Giosan et al., 2012). Thirteen samples from the top 120 cm (Unit I and II) of the GGC 18 core were dated using radiocarbon dating of bulk sediment (Coolen et al., 2009). In order to build an age model of the complete sediment core and be consistent with the age model published by Coolen et al. (2009), we collected six 5 cc samples at depths of 131 cm, 153 cm, 162 cm, 206 cm, 262 cm and 334 cm for ^{14}C AMS dating of bulk organic carbon at the National Ocean Sciences Accelerator Mass Spectrometry (NOSAMS) at WHOI (Table 1; Fig. S2). We calibrated these six new dates from Unit III of the Black Sea using the IntCal13 curve (Reimer et al., 2013), and calibrated the thirteen published dates from Unit I and II of the Black Sea (Coolen et al., 2009) using the Marine13 curve from the Bacon 2.2 package (Blaauw and Christen, 2011) taking into consideration the ^{14}C reservoir age offsets from Yanchilina et al. (2017) (Table 1).

2.3. Sample preparation and analysis of alkenones by GC-FID and GC-MS

All sediment samples were processed following established methods (e.g. Zheng et al., 2017). The samples were freeze-dried and extracted with a Dionex accelerated solvent extraction (ASE) system. After extraction, alkenones and alkenoates were isolated from total extracts using a silica gel column (SiO_2, 40-63 µm). The DCM fractions were further cleaned up using a silver thiolate silica gel column in a glass pipette (Wang et al., 2019; Zheng et al., 2017). We focused on analyses of alkenones in this study and did not quantify alkenoates, because some alkenoates eluted in different solvent fractions during silver thiolate silica gel separations. GC-FID analyses were performed using an Agilent 7890N Series instrument fitted with a Restek RTX-200 GC column (105 m $\times$ 250 µm$\times$ 0.25 µm) (Zheng et al., 2017). The structures of the alkenones/alkeonates were confirmed using an Agilent 6890 – 5973N GC-MS system.

2.4. RIK_{37}, C_{38Me}/C_{38Et} ratio, and %C37:4

The ratio of C_{37} isomeric ketones, or RIK_{37} (Longo et al., 2016), is computed as $C_{37:3a}/(C_{37:3a} + C_{37:3b})$, where $C_{37:3a}$ is the tri-unsaturated C_{37} alkenone with the double bond positions at $\Delta^{7,14,21}$ and $C_{37:3b}$ is the tri-unsaturated C_{37} alkenone with the

Table 1
Radiocarbon and calendar ages determined from bulk organic matter in 19 samples of GGC18. Reservoir ages are from Yanchilina et al. (2017). The date at the depth of 123 cm is excluded in the age model due to ^{14}C age reversal.

Depth (cm)	Unit	^{14}C age	^{14}C age error	Calibr. age	Calibr. age error	^{14}C reservoir (yrs)
2.5	I	1060	30	214	361	460
22.5	I	1910	30	1029	101	437
34.5	I	2390	30	1465	99	435
36.5	I	2450	25	1671	78	435
40.5	I	2890	30	2084	97	439
44	I	3120	35	2369	96	418
46	I	3150	35	2499	108	418
59	II	3700	30	3169	149	413
69	II	4200	30	3764	130	391
83	II	4990	30	4825	270	378
107	II	6420	30	6524	228	351
114	II	6840	40	6980	142	342
116	II	6910	30	7119	100	341
123	***III***	***9680***	***40***	-	-	-
131	III	9230	40	8886	348	1074
153	III	10750	50	12852	320	38
162	III	11650	70	13124	182	648
206	III	12550	85	14284	380	281
262	III	13450	90	15155	465	788
334	III	14600	110	16037	451	1704

double bond positions at $\Delta^{14,21,28}$. C_{38Me}/C_{38Et} ratios are computed by dividing the concentration of C_{38} methyl ketones by the concentration of C_{38} ethyl ketones. %C37:4 refers to the percentage abundance of $C_{37:4}$ alkenone relative to the sum of $C_{37:2}$, $C_{37:3}$ and $C_{37:4}$ alkenones: $\%C37{:}4 = C_{37:4}/(C_{37:2} + C_{37:3} + C_{37:4})$. In general, the order of %C37:4 in different groups of Isochrysidales is: Group I (>50 to 60%) > Group II (~5 to 50%) > Group III (<5%).

3. Results

3.1. Alkenone and alkenoate distributions in different units of Black Sea sediment core

In the present study, we analyzed alkenones and alkenoates in all three Units of the Black Sea sediments. Coolen et al. (2009) studied haptophyte biomarkers (i.e., ancient DNA and alkenones) from the same core but only from the organic-rich sediments of Units I and II. In a broader ancient DNA survey, these authors reported ancient plankton DNA (incl. trace amounts of Group III Isochrysidales) in Unit III sediments as old as 9.4 ka BP but alkenones were not studied in parallel (Coolen et al., 2013). This study is the first report of the alkenones and alkenoates in the Unit III sediments, as a result from application of a new suite of analytical methods (Wang et al., 2019; Zheng et al., 2017). Notably, alkenone concentrations are 20 - 384 μg/gdw (gram dry weight) in Unit I, 33 – 230 μg/gdw in Unit II and in much lower concentration of 0 – 35 μg/gdw in Unit III sediments (Fig. S3).

Alkenone and alkenoate profiles show distinctive changes at different depths and units in the GGC18 core (Fig. 1). Based on the culture experiments and comprehensive compilation of published culture data (Zheng et al., 2019), we divide succession of alkenone and alkenoate distributions in GGC18 into six distinct phases (Fig. 1):

Phase I (334 – 123 cm; ~ 16.6 to 7.6 ka BP): The distinctive feature of this phase is the presence of double bond positional isomers for C_{37} and C_{38} alkenones (Dillon et al., 2016), and absence or very low concentration of alkenoates (Fig. 1f). The ratio of C_{37} isomers, RIK_{37} (Longo et al., 2016), shows relatively low values around 16 ka BP, but increasing slowly to 1 around the Unit III to II boundary at 7.6 ka. The ratio of C_{38} methyl over C_{38} ethyl alkenones is ~ 0.5 at 16.5 ka, but steadily decreases to ~ 0.1 at the Unit III – II boundary at 7.6 ka (Fig. 2). %C37:4 is 15 to 55%, with highest values around 15 ka (Fig. 3d).

Phase II (123 to 113 cm; ~7.6 to 6.9 ka BP): Around the boundary of Unit II and Unit III (123 cm), we found a section of distinctive alkenone distributions between 123 to 108 cm, characterized by very low C_{38} Me/C_{38} Et ratios (~ 0.05), with a near absence of tri-unsaturated C_{37} and C_{38} alkenones but presence of alkenoates (Fig. 1e). This alkenone/alkenoate profile is consistent with a predominance of Group II haptophytes (Zheng et al., 2019).

Phase III: Group III *E. huxleyi* type alkenones were found between 113 to 66 cm depth (or 6.9 to 3.5 ka BP) (Fig. 1d), with the presence of both C_{38} methyl to C_{38} ethyl alkenones and absence of $C_{37:3}$ isomer. The C_{38}Me/C_{38}Et ratio is relatively high (0.9 to 0.5), suggesting a relatively high salinity level (> 11 psu).

Phase IV (66-42 cm; 3.5-2.2 ka BP): A change in the alkenone profile occurs at 66 cm, 3.5 ka (Fig. 1c), where *E. huxleyi* type alkenones are replaced by the very unusual type of ethyl alkenones possessing double bond positions at $\Delta^{14,19}$ (conventional di-unsaturated alkenones have double bonds at $\Delta^{14,21}$), with the most abundant homologue being $C_{36:2}$Et (Fig. 1c; Xu et al., 2001). Tri-unsaturated alkenones are generally absent in this interval. The most important feature of alkenones in this horizon is the absence of C_{38}Me or C_{39}Et. This feature is consistent with Group II, brackish alkenone producers (Zheng et al., 2019). These unusual shorter chain alkenones have been proposed to be biosynthesized through β oxidation of Δ^{21} monounsaturated parent alkenones, followed by desaturation at Δ^{14} (Zheng et al., 2016). They have been previously found in the Baltic Sea (e.g., Warden et al., 2016), and the Florida Bay (van Soelen et al., 2014) where salinity is significantly lower than open ocean. Notably, the structures of these Black Sea shorter chain alkenones differ from shorter chain alkenones (double bond positions at $\Delta^{12,19}$, with both methyl and ethyl substitutions for C_{38} alkenone derivatives) produced by a mutant species of *E. huxleyi* (Prahl et al., 2006). Biosynthetically, Zheng et al. (2016) proposed that *E. huxleyi* type shorter chain alkenones are produced by β oxidation of $\Delta^{14,21}$ di-unsaturated parent alkenones.

Phase V (42 – 36 cm; 2.2 to 1.6 ka BP): The shorter chain type of alkenones were gradually replaced by regular brackish Group II alkenones at ~42 cm. C_{38} Me and C_{39} Et are still absent, alkenoates are abundant (Fig. 1b), whereas %C37:4 is 15 to 20 (Fig. 3d). This is the period of the transitional sapropel between the first invasion and the initiation of final invasion of coccolithophore

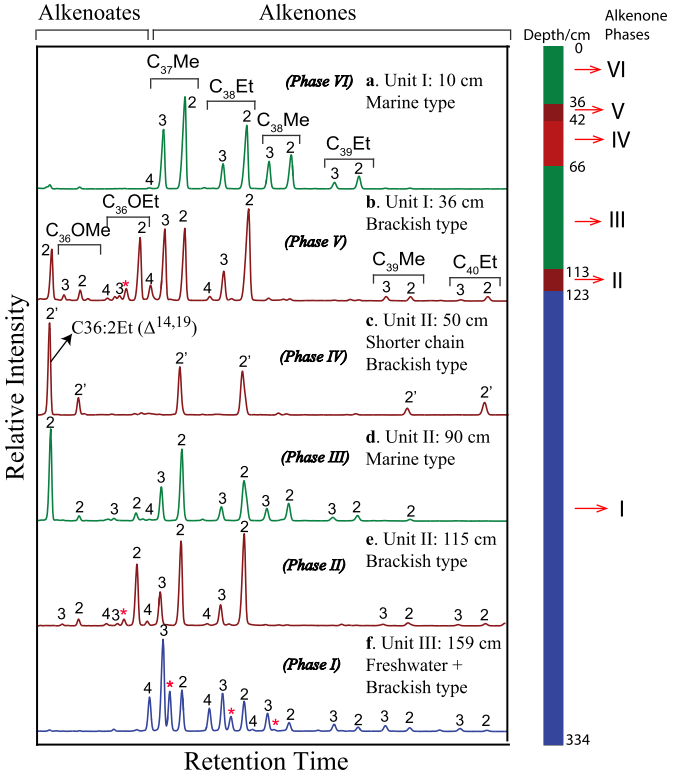

Fig. 1. Examples of GC-FID chromatograms for the six typical phases (a to f) of long chain alkenones and alkenoates in the GGC18 sediment samples of the Black Sea, deposited over the past 16.6 kyr. The depth ranges (Phase I: 334-123 cm or 16.6 to 7.6 ka BP; Phase II: 123-113 cm or 7.6 to 6.9 ka BP; Phase III: 113-66 cm or 6.9 to 3.5 ka BP; Phase IV: 66-42 cm or 3.5-2.2 ka BP; Phase V: 42-36 cm or 2.2 to 1.6 ka BP; Phase VI: 36-0 cm or 1.6 ka BP to present) of the six phases in core GGC18 are graphically depicted and proportionally marked on vertical column on the right of the exemplary chromatograms. The chain length of alkenones and alkenoates ranges from C_{37} to C_{40}. Alkenones are designated with C_nMe or C_nEt, where n is the carbon number, and Me and Et represent methyl and ethyl alkenones respectively. Similarly, Alkenoates are designated with C_{36}OMe or C_{36}OEt where OMe and -OEt are methyl and ethyl esters respectively. Numbers 4, 3 and 2 on top of individual peaks denote the number of double bonds. 3a and 3b are tri-unsaturated double bond positional isomers. The double bonds number 2' for the alkenones and alkenoates in the Phase IV represents the shorter chain alkenones with double bond positions at $\Delta^{14,19}$. Phase V is the transitional sapropel layer defined in Hay et al. (1991). (For interpretation of the colors in the figure(s), the reader is referred to the web version of this article.)

E. huxleyi in the Black Sea (Hay et al., 1991), indicating Group II Isochrysidales species were predominant producers of alkenones (Zheng et al., 2019; Kaiser et al., 2019).

Phase VI (36 – 0 cm; 1.6 ka BP to present): Alkenones in this interval are similar to those in Phase III. The relatively high abundance of C_{38}Me and C_{39}Et indicates that the dominant alkenone-producing haptophyte was the Group III marine haptophyte *E. huxleyi* (green profile; Fig. 1a), consistent with *sed* aDNA data (Coolen et al., 2009).

3.2. Ratio of C_{38} methyl and C_{38} ethyl alkenones

Group II brackish haptophytes do not produce (or only produce very trace amounts of) C_{38} methyl alkenones (hence this ratio is ~zero), whereas Group III marine haptophytes (*E. huxleyi* mainly) have high values (0.6 to 0.9), and Group I haptophytes intermediate values (~0.5) (Zheng et al., 2019; Kaiser et al., 2019). Because Group I Isochrysidales occurs in freshwater and oligohaline environments (Longo et al., 2016), it is most likely to mix with Group II in low salinity brackish waters. Similarly, Group III can mix with Group II in brackish environments such as the Baltic Sea (Kaiser et al., 2019). Therefore, C_{38}Me/C_{38}Et ratio (Fig. 2d) can be used to assess the degree of mixing for all three different Isochrysidales groups, and subsequently to constrain salinity ranges.

In Unit III of the Black Sea (alkenone Phase I), the ratio of C_{38}Me/C_{38}Et fluctuates around 0.25-0.5 between 16.3 and 14 ka, then decreases progressively to nearly zero at the Unit III and II boundary, 7.6 ka (Fig. 2d). Because all samples in this interval contain tri-unsaturated alkenone isomers, and C_{38}Me/C_{38}Et ratio is below 0.5, this is a clear case of mixing of Group I and Group II alkenones. The relative contributions from Group II increasing from 16 ka to the Unit III and Unit II boundary, suggesting slowly rising salinity. Mixing of Group I and II Isochrysidales is also illustrated by significant correlation between RIK_{37} and C_{38}Me/C_{38}Et ratios in the Unit III sediment (Fig. S4). Between 7.6 ka and 6.9 ka (alkenone Phase II), the ratio of C_{38}Me/C_{38}Et is close to 0 and alkenoates are present. This profile indicates that the Group II haptophytes were the dominant alkenone producer. C_{38}Me/C_{38}Et alkenone ratio increases abruptly from 0 to 0.9 at 6.9 ka, then decreased progressively to ~ 0.5 at 3.5 ka. This pattern is consistent with dominant input by marine Isochrysidales (*E. huxleyi*) during this interval (alkenone Phase III). This is in agreement with a gradual replacement of freshwater by marine plankton through non-specific parallel *sed* aDNA profiling of eukaryotes in general (Coolen et al., 2013). Around the boundary of Unit I/II, there is an interval (1.6 ka to 3.5 ka, alkenone Phase IV and V) with dominant input from Group II brackish haptophytes as the ratio of C_{38}Me/C_{38}Et is close to 0. At 1.6 ka, marine Group III alkenones replaces the brackish Group II alkenones abruptly and remains dominant until present (alkenone Phase I).

3.3. Paleosalinity of Unit III

RIK_{37} has been proposed as a salinity indicator for fresh to oligohaline waters since this ratio is not temperature sensitive (Longo et al., 2016). A surface sediment calibration of the RIK_{37} index in the freshwater and brackish Baltic Sea yielded the following correlation with salinity: $RIK_{37} = 0.0677^{*}$ salinity + 0.532; $R^2 = 0.7$, RMSE = 0.914 psu (Kaiser et al., 2019). Baltic Sea salinity changes gradually from 0 to 35 psu, with broad regions of relatively uniform mean salinity levels for comparison with alkenone distributions. As we expected, RIK_{37} value increases with salinity as the contribution from Group II haptophytes increase relative to Group I haptophytes (Fig. 2).

Between 16.6 and 13 ka, RIK_{37} averages around 0.7 with high frequency fluctuations between ~0.6 to 0.8. This RIK_{37} range indicates oligohaline waters with surface salinity fluctuating between 1 to 3 psu in the Black Sea. From 13 ka to the Unit III/II boundary at 7.6 ka (alkenone Phase I), gradually increasing RIK_{37} ratios signify a slowly rising salinity from 2 to 6 psu. Following the termination of Unit III at 7.6 ka and between 7.6 and 6.9 ka (alkenone Phase II), RIK_{37} stays high (fluctuating between 0.95 to 1), suggesting a brackish water environment with salinity occasionally higher than 6 psu. This RIK_{37} inferred salinity level is consistent with the brackish conditions inferred from C_{38}Me/C_{38}Et ratios, whose decreasing trend from 16.6 to 6.9 ka is consistent with increasing Group II relative to Group I haptophytes (Zheng et al., 2019; C_{38}Me alkenones are produced by Group I but not Group II haptophytes) (Fig. 2). The RIK_{37} ratio for the past 6.9 kyr is 1, indicating the salinity has exceeded the maximal tolerance level for Group I haptophytes (~ 6 psu; Longo et al., 2016; Fig. 2a, b, c).

4. Discussions

4.1. Black Sea lake salinity during the deposition of Unit III: 16.6 – 9.4 ka BP

This phase of the Black Sea represents Unit III deposition before IMI. The IMI has been identified to occur at ~ 8.5-9.4 ka, depend-

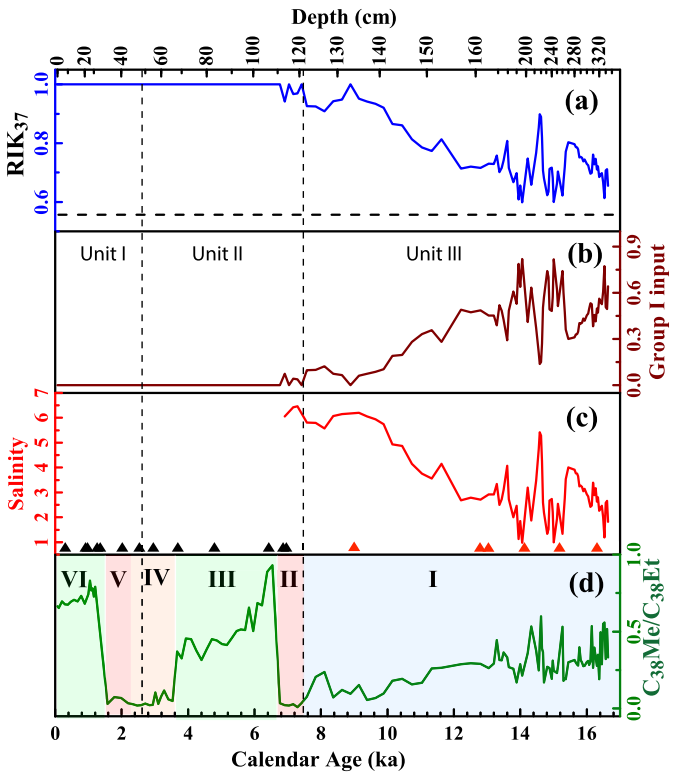

Fig. 2. (a) RIK_{37} record for GGC 18 core; (b) relative Group I input computed based on the linear scaling of RIK_{37}, assuming two endmembers: $RIK_{37} = 0.55$ when Group I Isochrysidales input is 100%, and $RIK_{37} = 1$ when Group I input is zero; (c) reconstructed salinity based on Baltic Sea salinity calibration (Kaiser et al., 2019). Marine regressions and transgressions during the glacial and interglacial cycles in Baltic Sea have similar characteristics to those in Mediterranean and Baltic Sea. Therefore, the RIK_{37}-salinity calibration developed in Baltic Sea is likely well suited for reconstructing Black Sea salinity changes; (d) Variations in the ratio of C_{38}Me and C_{38}Et for GGC 18. All data points are plotted against calendar ages. Black triangles are radiocarbon dates from Coolen et al., 2009; the red triangles are the new radiocarbon dates from this study.

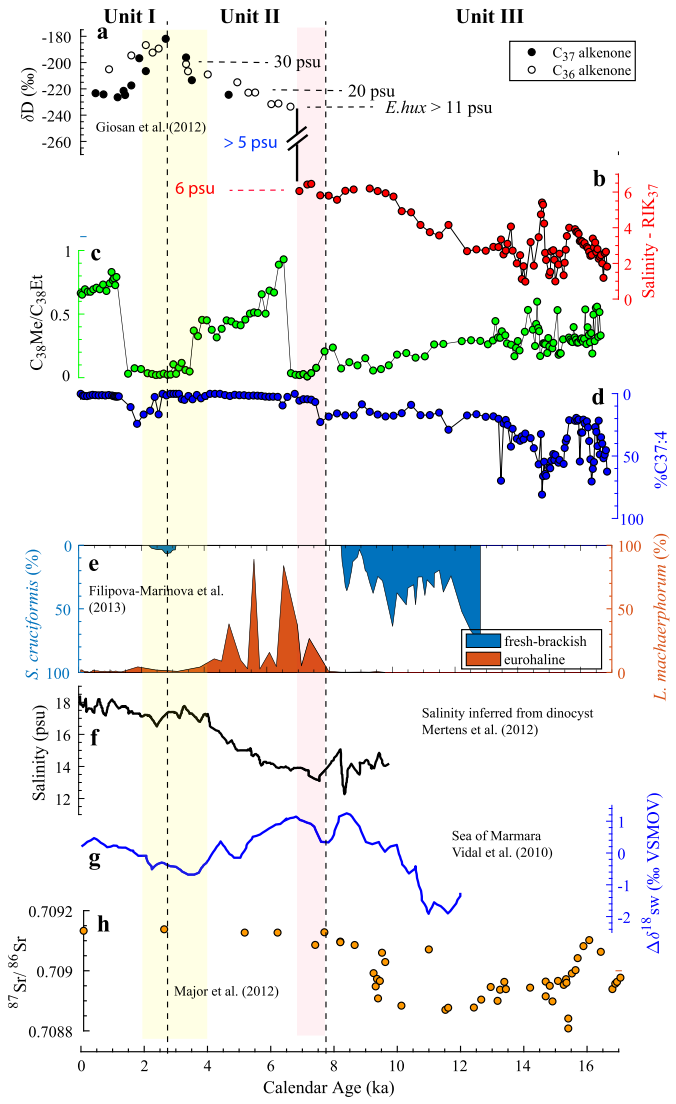

Fig. 3. Various proxy records of the Black Sea salinity for the past 16.6 kyr: (a) δD values of C_{37} and C_{36} alkenones from GGC18 and inferred salinity record (Giosan et al., 2012), (b) RIK_{37}-inferred salinity for GGC18; (c) ratio of C_{38Me}/C_{38Et}; (d): percentage of C37:4 alkenones; (e) records of fresh-brackish dinocyst *S. cruciformis* (3 - 7 psu) and eurohaline *dinocyst L. machaerophorum* (>10 psu) from Filipova-Marinova et al. (2013); (f) dinocyst-assemblage inferred salinity from Mertens et al. (2012), (g) δ^{18}O values of seawater reconstructed based on planktonic foraminifera from the Marmara Sea (Vidal et al., 2010); (h): $^{87}Sr/^{86}Sr$ record from Major et al. (2006). IMI refers to Initial Marine Input, as defined by Major et al. (2006).

ing on variable reservoir age corrections (Coolen et al., 2013; Herrle et al., 2018; Major et al., 2006; Soulet et al., 2011; Yanchilina et al., 2017; Ankindinova et al., 2019). To simplify our discussion, we define the timing of the IMI to 9.4 ka, based on combined evidence of strontium isotope excursion (Fig. 3h; Major et al., 2006) and parallel *sed* aDNA profiling performed on this core (Coolen et al., 2013).

Our RIK_{37} record suggests an overall progressively rising salinity from 16.6 to 9.4 ka, ranging from 1 to 6 psu (Figs. 2c & 3b), which is in good agreement with published results. For example, the chloride content and δ^{18}O values of sediment interstitial water suggest that in this late glacial period the Black Sea lake was fresh with salinity $\sim$ 1 psu (Soulet et al., 2010). Similarly, Yanchilina et al. (2017) found that the entire mollusk assemblage in the cores on the shelf was composed of oligohaline species, indicating the salinity in Unit III was in the range of 1 to 5 psu. Filipova-Marinova et al. (2013) analyzed the same sediment core as used in the present study, and observed fresh- to brackish-water species (i.e., *Spiniferites cruciformis* and *Pyxidinopsis psilata*) dominant in the dinoflagellate cyst assemblage in the Unit III sediment from 12 to 7.6 ka (Fig. 3e). Mudie et al. (2004) associated *Spiniferites cruciformis* with low salinity (3-7 psu), oligohaline waters. Recent data based on ostracode species also indicate a low salinity (5 – 8 psu) during the last glacial maximum, but with lower salinity (0 – 5 psu) during the first Meltwater Pulse during Heinrich Stadial 1 (Briceag et al., 2019).

Between 16.6 and 13 ka, both the RIK_{37} and C_{38}Me/C_{38}Et ratios indicate large salinity fluctuations between fresh and oligohaline waters in the Black Sea (Fig. 4). Such rapid fluctuations between fresh and oligohaline conditions are likely related to major pulses of meltwater inputs to the Black Sea from the Fennoscandian Ice Sheet (FIS), the world's second largest ice sheet at the time, and icecaps at the Alps (Major et al., 2006; Soulet et al., 2013; Yanchilina et al., 2019). During the deglaciation, these continental ice formations have been suggested to strongly affect the Black Sea salinity by discharging freshwater via the Danube, Berezina and Dniepr Rivers (Soulet et al., 2013; Yanchilina et al., 2019). Specifically, Soulet et al. (2013) found periods of strong meltwater pulses by using the BIT (branched and isoprenoid tetraether) index and C_{25} *n*-alkane/TOC ratios, and neodymium isotopes (Fig. 4b, c, d). Yanchilina et al. (2019) demonstrated that massive amounts of melt water (>25,000 km^3) along with red-brown clay were delivered to Black Sea lakes between 16.35 and 15.4 ka BP. We find periods of low salinity as inferred from RIK_{37} and C_{38}Me/C_{38}Et ratios (Figs. 4a, 4b; Fig. S4), which show general overlap with inferred

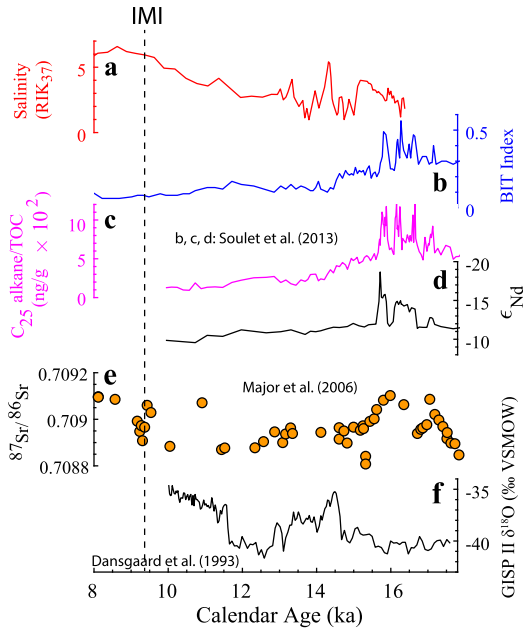

Fig. 4. Comparison of the RIK_{37}-reconstructed salinity from GGC18 with other proxy records between 8 and 16.6 ka; (a) deglaciation meltwater records from Soulet et al. (2013), where b, c, d refer to BIT, or branched vs isoprenoid tetraether index, TOC-normalized C_{25} *n*-alkane abundance, and epsilon Nd, respectively; (e) strontium isotope record from Major et al. (2006); (f) GISPII ice core $\delta^{18}O$ record (Dansgaard et al., 1993). IMI refers to Initial Marine Input, as defined by Major et al. (2006).

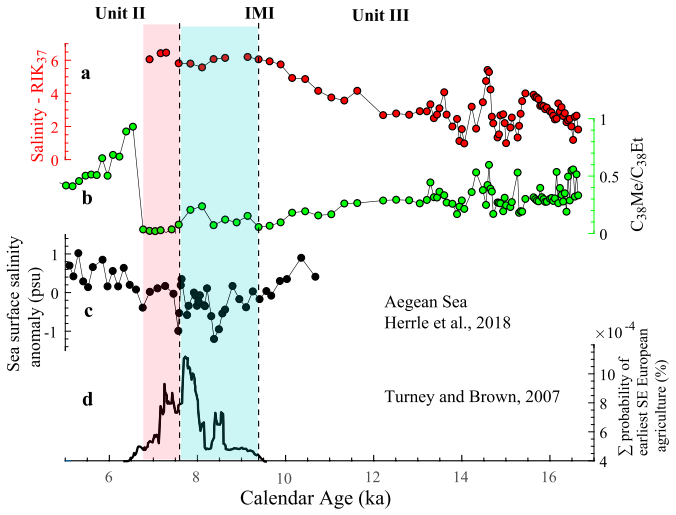

Fig. 5. (a) Sea surface salinity variation of the Black Sea reconstructed from RIK_{37}; (b) record of $C_{38}Me/C_{38}Et$ ratio of the Black Sea; (c) record of salinity anomaly from Aegean Sea based on phytoplankton transfer function (Herrle et al., 2018); (d) combined records for the establishment of Neolithic farmers across southeastern Europe during the Holocene (Turney and Brown, 2007). IMI refers to Initial Marine Input, as defined by Major et al. (2006).

stronger meltwater pulses (Soulet et al., 2013), and/or strontium isotope fluctuations (Fig. 4e; Major et al., 2006). We therefore surmise that the gradually rising salinity level after 13 ka until the time of IMI at 9.4 ka in the Black Sea (Coolen et al., 2013) is due to a regional negative hydrological balance, leading to the evaporative enrichment of salt content in the Black Sea lake.

Our RIK_{37} and $C_{38}Me/C_{38}Et$ records do not display any sign of salinity reversal associated with the Younger Dryas (12.9 to 11.7 ka) cold interval as the Black Sea surface salinity continued to climb by ~ 2 psu during this time (Figs. 4). Similar (i.e., small increasing) trend is also recently proposed by Briceag et al. (2019) based on ostracode assemblages. This suggests that the overall hydrological balance in the Black Sea basin did not show abrupt changes during this episode. We do observe, however, a relatively large increase in Black Sea salinity (to ~ 4 psu) at ~ 14.7 ka during the Bølling/Allerød (Fig. 4). Warm and dry conditions at B/A period for the Mediterranean region would have caused the enhancement of the evaporation/precipitation (E/P) ratio, which reduced the river runoff of the Black Sea catchment as well (Fig. 3g; Vidal et al., 2010). Our data are consistent with the records of regional hydrological balance suggesting that, prior to 14.7 ka (23 to 14.7 ka), the Black Sea catchment has a relatively high P-E and was overflowing to the Marmara Sea: similar $\delta^{18}O$ values of carbonate in the Black Sea and the Marmara Sea support their surface water connectivity (Figs. 3 & 4; Bahr et al., 2006; Vidal et al., 2010).

4.2. Black Sea lake salinity variations between 9.4-7.6 ka

From 9.4 (IMI) to 7.6 ka (the start of sapropel deposition), the Black Sea surface salinity was in the range of 5 to 6 psu (near the upper limit of the RIK_{37} index; Fig. 3 & 5). The relatively low surface salinity during this interval is surprising, since strontium isotope data (Major et al., 2006; Ankindinova et al., 2019) and an increase in the relative abundance of *sed* aDNA from marine eukaryotes (Coolen et al., 2013), clearly indicate the introduction of Mediterranean Sea water (Fig. 5). However, quantitative salinity data cannot be inferred from these geochemical and genomic markers and we attribute the low salinity of the Black Sea during this time interval to a major increase in regional hydrological balance. Positive regional hydrological balance is supported by recently published record of Aegean Sea salinity anomaly by Herrle et al. (2018), indicating freshening of the Aegean Sea surface water from 11 to 7.6 ka (Fig. 5).

Our data may imply the inflow of marine water to the Black Sea starting from 9.4 ka coincided with major rise in regional rainfall, leading to a subdued salinity level of the Black Sea surface water. At present, the Black Sea is connected with the Marmara Sea through the Bosporus Strait, which is 30 km long with a maximum width of 3.7 km and minimum width of 750 m, and a depth ranging from 36.5 to 124 m (Fig. S1). On the surface and particularly in the center of the Bosporus strait, there is a rapid current flow from the Black Sea to the Marmara Sea, but a countercurrent below the surface carries water of greater density from the Marmara Sea to the Black Sea. We surmise similar configuration may have existed between 9.4 and 7.6 ka.

We note the rise of the earliest southeastern European agriculture starts from ~ 9.6 ka (Turney and Brown, 2007), peaking at around 7.6 ka (Fig. 5), consistent with our hypothesis of greatly enhanced regional rainfall in the catchment of the Black Sea. The sea level rise resulting from retreat and collapse of the Laurentide Ice Sheet may have caused flooding of coastal areas of the Black Sea, leading to the sudden loss of land favored by early farmers and initiated an abrupt expansion of migrating Neolithic peoples across Europe.

4.3. Mid to late Holocene (Unit I and II): 7.6 ka to present

There was a transition period from 7.6 to 6.9 ka characterized by brackish type Group II alkenones with low $C_{38}Me/C_{38}Et$ ratio, and occasionally Group I alkenones were also present (alkenone phase II; Figs. 2e & 3). *E. huxleyi* only became the dominant haptophyte from 6.9 ka, with a sudden jump of $C_{38}Me/C_{38}Et$ ratio (alkenone phase III; Fig. 2d). As the minimal threshold salinity for *E. huxleyi* observed in modern ocean is ~ 11 psu (Coolen et al., 2013), our results imply that the Black sea surface salinity ranged from 6 to 11 psu between 7.6 to 6.9 ka. The relatively low salinity during this 700-year interval is surprising, since the Black Sea was already fully connected with the Mediterranean Sea. Possible

reasons for the relatively low surface salinity in the Black Sea between 7.6 and 6.9 ka include high influx of river run-off due to the positive regional hydrological balance, with high salinity waters flowing into the Black Sea as a bottom current through the Bosporus. As a result, the Black Sea surface salinity may have not increase dramatically until sufficient amounts of saline water had been mixed from bottom up.

Published salinity reconstructions in the past 7.6 kyr have considerable disagreements, depending on proxies used (Aksu et al., 2002; Giosan et al., 2012; Mertens et al., 2012; van der Meer et al., 2008). The most recent Black Sea salinity reconstruction for the past 7.2 kyr is based on alkenone δD values. The δD values of C_{37} and C_{36} alkenones suggest a progressive increase in salinity from 6.8 to 2.6 ka to a maximum above 30 psu (but note δD data are absent between 3.1 and 2.6 ka), followed by a subsequent progressive freshening of surface water to 19 psu (Fig. 3a; Coolen et al., 2013; Giosan et al., 2012; van der Meer et al., 2008). However, the alkenone hydrogen isotope-based salinity reconstruction disagrees with more conventional records. For example, sedimentological and paleontological data do not suggest peak salinity at $\sim$ 2.5 ka and there is no evidence for progressive freshening of surface water during the late Holocene interval of coccolith deposition (Unit I) (Fig. 3; Aksu et al., 2002; Mertens et al., 2012). Filipova-Marinova et al. (2013), using the exact same sediment core, GGC 18, as used in our study and used for hydrogen isotope analysis (Giosan et al., 2012), found an increase in fresh- to brackish- water dinoflagellates (e.g., *Spiniferites cruciformis* and *Pediastrum simplex var. simplex*) around 2.7 ka BP, when the percentage of the euryhaline marine species (e.g., *Lingulodinium machaerophorum*) greatly diminished, even disappeared (Fig. 3e). This period of decrease in surface salinity is attributed to increased river inputs into the Black Sea from Danube, Dniester, Dnieper and Don (Filipova-Marinova et al., 2013). Therefore, the results from dinoflagellate assemblages support an opposite conclusion as inferred from alkenone hydrogen isotopic ratios, i.e., there is a salinity *trough*, rather than a peak, around 2.7 ka in the mid to late Holocene, although the absence of alkenone δD measurements between 3.1 and 2.6 ka (Giosan et al., 2012) may have contributed to the discrepancies.

Our comprehensive alkenone and alkenoate profiling in Phases IV and V is consistent with dinoflagellate-based salinity reconstruction indicating significant surface water freshening between 3.5 and 1.6 ka (Fig. 3e, f; (Filipova-Marinova et al., 2013; Mertens et al., 2012). Between 3.5 and 1.6 ka, there was a major change in haptophyte speciation in the Black Sea: the prior dominance of marine *E. huxleyi* type alkenones was replaced by Group II brackish haptophytes (Fig. 3c, d). This interval stratigraphically matches the interval of the disappearance (after a brief initial appearance) of *E. huxleyi* coccolith fossils, and is termed the "Transition sapropel" layer (2.7 – 1.6 ka) (Hay et al., 1991; Jones and Gagnon, 1994), suggesting a reduced salinity that impeded growth of *E. huxleyi*. This contradicts the results of our parallel *sed* aDNA study, which revealed that *E. huxleyi* was the sole source of alkenones during the transition sapropel (Coolen et al., 2013). Interestingly, a more in depth parallel *sed* aDNA survey from this core GGC18 with the aim to elucidate 7000 years of co-evolution of *E. huxleyi* and its coccolithoviruses, revealed the development of a unique *E. huxleyi* genotype that most likely represented a non-calcified strain that escaped prior microscopic detection in the transition sapropel (Coolen, 2011). Namely, coccolithoviral infection requires the presence of a calcified stage and coccolithoviral DNA was only absent in this coccolith devoid transition sapropel (Coolen, 2011). Our current study shows that reduced rather than maximum salinity must have selected for this non-calcified *E. huxleyi* that co-existed with a predominance of previously overlooked (the detection approach may have been too specific) non-calcified Group II Isochrisadales as the main source of alkenones. Salinity minima at $\sim$ 3.5 to 1.6 ka in the Black Sea in the past 6.8 kyr is also supported by reconstruction from the Marmara Sea based on planktonic foraminifera δ^{18}O values and alkenone inferred SST (Fig. 3g; Vidal et al., 2010). The estimated δ^{18}O of seawater at the Marmara Sea shows a period of lower values from 2 to 4 ka BP, suggesting this period was the freshest in the Marmara Sea during the Holocene (Vidal et al., 2010). Many studies (e.g., Aksu et al., 2002 and references therein) have suggested a constant outflow of Black Sea surface water to the Marmara Sea in the past 6.8 kyr. Combining all the evidence above, we conclude that the Black Sea surface water experienced a period of low salinity between 3.5 and 1.6 ka, probably as a result of major increase in regional hydrological balances.

Our alkenone and alkenoate profiles in Phase IV and Phase V also provide a rational explanation for results from alkenone δD measurements (Fig. 1). Culture growth experiments using *E. huxleyi* and *I. galbana* have found large differences in hydrogen isotope fractionation values, with the later brackish Group II haptophyte fractionating by 50 - 100‰ less than *E. huxleyi* (M'boule et al., 2014; Chivall et al., 2014). Therefore, the unusually high δD values of alkenones between 3.5 and 1.6 ka primarily originated from changes in the dominant alkenone-producing haptophytes. When the salinity reconstructions reported by van der Meer et al. (2008) and Giosan et al. (2012) are corrected using an average 75‰ fractionation factor difference (estimated based on M'boule et al., 2014), there would be an isotopic minimum between 3.5 – 1.6 ka. Because growth rates and other environmental factors can strongly affect the specific isotopic fractionation factors (M'boule et al., 2014; Chivall et al., 2014), we cannot quantitatively reconstruct the salinity during this interval, unfortunately.

4.4. Rate of surface salinity changes during marine transgression

Neither RIK_{37} nor $C_{38}Me/C_{38}Et$ indices display abrupt sea surface salinity changes at the time of IMI at 9.4 ka (Figs. 2 & 4). We do not see an abrupt replacement of freshwater and brackish water Group I and Group II alkenones by the marine Group III alkenones at the Unit III and II boundary (7.6 ka). Instead, from 7.6 to 6.9 ka, we observe a persistence of Group II brackish water alkenones for $\sim$ 700 years between 7.6 and 6.9 ka (Fig. 2), before the complete and abrupt change to marine Group III alkenones.

Absence of abrupt surface salinity changes inferred by alkenone profiles also agrees with our parallel *sed* aDNA study targeting eukaryotes (Coolen et al., 2013), and the recent salinity reconstruction from the Aegean Sea (Herrle et al., 2018), suggesting gradually declining surface water salinity between 9.4 and 6.9 ka (Fig. 5). Freshening in the Aegean Sea could only occur if the surface input from the Black Sea and the Marmara Sea had lower salinity values during this interval. Relatively low salinity in the Black Sea surface waters between 9.4 and 6.9 ka, which is counter-intuitive given this is the time when the Black Sea lake reconnected with the salty Mediterranean Sea water, would have only been possible if there was a major increase in the hydrological balance in the Black Sea catchment (Herrle et al., 2018; Ankindinova et al., 2019). The increase in precipitation and the consequent river runoff, coincidentally, drove major agricultural innovations in the southeastern Europe (Fig. 5; Turney and Brown, 2007). We note that Aksu et al. (2002), Hiscott and Aksu (2002) and Mudie et al. (2004) have also presented evidence that there was persistent outflow of brackish water from the Black Sea into the Marmara Sea before the global sea level reached the Bosporus sill at early Holocene, and therefore marine transgression of the Black Sea was a gradual process with seawater mixing slowly with the Black Sea Lake through the bottom water flows.

5. Conclusions

Detailed alkenone and alkenoate analysis reveals a complex history of Isochrysidales species successions in the past 16,000 years in the Black Sea. For the first time, alkenones are found throughout the Unit III sediment of the Black Sea using a new suite of analytical methods. The Unit III alkenones contain variable mixture of Group I and Group II alkenones, allowing the use of RIK_{37} and $C_{38}Me/C_{38}Et$ indices to quantitatively assess the salinity history. From 16.6 to 9.4 ka, we show that the Black Sea lake evolved from a near freshwater to oligohaline lake ($\sim$ 5 psu). The overall increase in salinity in the closed basin lake during this deglacial period suggests a negative regional hydrological balance in the Black Sea catchment. Deglacial meltwater pulses from Fennoscandian Ice sheet may have served as key freshwater inputs to reduce the Black Sea surface salinity between 16.6 and 14 ka.

The Black Sea surface salinity remained subdued around 6-7 psu between IMI (9.4 ka) and Unit II and III depositional boundary (7.6 ka). In fact, brackish water conditions (7 – 11 psu) persisted for another 700 years post Unit II and III boundary. Together with the most recent evidence indicating freshening Aegean Sea and major rise of agricultural activities in the southeastern Europe during this interval, we conclude a major increase in regional hydrological balance in the Black Sea catchment is the culprit for maintaining the relatively low surface salinity conditions of the Black Sea. Our salinity reconstructions are inconsistent with an abrupt surface salinity rise at the time of reconnection ($\sim$ 9.4 ka) between the Mediterranean Sea and the Black Sea through Bosporus sill. More saline, near modern surface salinity was only attained later at $\sim$6.9 ka. We propose that the water exchange between the Black Sea and the Marmara Sea has already attained conditions similar to modern configurations between 9.4 and 7.6 ka.

In the past 6,900 years (Unit II and I), we identified one period of time lasting 1,900 years between 3.5 to 1.6 ka, when Black Sea surface water salinity declined significantly, allowing Group II Isochrysidales to become the dominant alkenone producer. This period partially overlaps with the transitional sapropel layer previously identified (Hay et al., 1991; Jones and Gagnon, 1994; Ross and Degens, 1974). Our proposal contradicts with earlier salinity reconstruction based on alkenone hydrogen isotopic values, which suggest that Black Sea salinity peaked at this interval. Absence of alkenone δD measurements between 3.2 and 2.6 ka, as well as the large differences in hydrogen isotope fractionation between Group II Isochrysidales and *E. huxleyi* readily reconcile the difference between inferred salinity levels based on alkenone/alkenoate profiles and alkenone hydrogen isotopic values. A combination of increased river inputs, regional runoff and higher regional P-E balance could have been the causes for this period of Black Sea salinity decrease.

CRediT authorship contribution statement

YH initiated this project and acquire the funding to support the research. LG and MC provided advise in sample selection. YZ and PH performed sample analyses. All authors discussed data interpretations. YH and YZ drafted the paper, which is further revised by all co-authors.

Declaration of competing interest

The authors declare that they have no known competing financial interests or personal relationships that could have appeared to influence the work reported in this paper.

Acknowledgements

This work was supported by the United States National Science Foundation awards to Y.H. (EAR-1122749, PLR-1503846, EAR-1502455; EAR-1762431), as well as seed funds from Institute at Brown for Environment and Society, Brown University (IBES). We thank Dr. A.G. Yanchilina for valuable comments and suggestions that helped improve our manuscript.

Appendix A. Supplementary material

Supplementary material related to this article can be found online at https://doi.org/10.1016/j.epsl.2021.116881.

References

Aksu, A.E., Hiscott, R.N., Kaminski, M.A., Mudie, P.J., Gillespie, H., Abrajano, T., Yasar, D., 2002. Last glacial Holocene paleoceanography of the Black Sea and Marmara Sea: stable isotopic, foraminiferal and coccolith\revidence. Mar. Geol. 190, 119–149.

Ankindinova, O., Hiscott, R.N., Aksu, A.E., Grimes, V., 2019. High-resolution Sr-sotopic evolution of Black Sea water during the Holocene: implications for reconnection with the global ocean. Mar. Geol. 407, 213–228.

Bahr, A., Arz, H.W., Lamy, F., Wefer, G., 2006. Late glacial to Holocene paleoenvironmental evolution of the Black Sea, reconstructed with stable oxygen isotope records obtained on ostracod shells. Earth Planet. Sci. Lett. 241, 863–875.

Ballard, R.D., Coleman, D.F., Rosenberg, G.D., 2000. Further evidence of abrupt Holocene drowning of the Black Sea shelf. Mar. Geol. 170, 253–261.

Blaauw, M., Christen, J.A., 2011. Flexible paleoclimate age-depth models using an autoregressive gamma process. Bayesian Anal. 6, 457–474.

Briceag, A., Yanchilina, A., Ryan, W.B.F., Stoica, M., Melinte-Dobrinescu, M.C., 2019. Late Pleistocene to Holocene paleoenvironmental changes in the NW Black Sea. J. Quat. Sci. 34, 87–100.

Chivall, D., M'Boule, D., Sinke-Schoen, D., Sinninghe Damsté, J.S., Schouten, S., van der Meer, M.T.J., 2014. Impact of salinity and growth phase on alkenone distributions in coastal haptophytes. Org. Geochem. 67, 31–34.

Coolen, M.J.L., 2011. 7000 years of *Emiliania huxleyi* viruses in the Black Sea. Science 333, 451–452.

Coolen, M.J.L., Orsi, W.D., Balkema, C., Quince, C., Harris, K., Sylva, S.P., Filipova-Marinova, M., Giosan, L., 2013. Evolution of the plankton paleome in the Black Sea from the deglacial to Anthropocene. Proc. Natl. Acad. Sci. USA 110. https://doi.org/10.1073/pnas.1219283110.

Coolen, M.J.L., Saenz, J.P., Giosan, L., Trowbridge, N.Y., Dimitrov, P., Dimitrov, D., Eglinton, T.I., 2009. DNA and lipid molecular stratigraphic records of haptophyte succession in the Black Sea during the Holocene. Earth Planet. Sci. Lett. 284, 610–621.

Dansgaard, W., Johnson, S.J., Clausen, H.B., Dahl-Jensen, D., Gundestrup, N.S., Hammer, C.U., Hvidberg, C.S., Steffensen, J.P., Sveinbjörnsdottir, A.E., Jouzel, J., Bond, G., 1993. Evidence for general instability of past climate from a 250-kyr ice-core record. Nature 364, 218–220.

Dillon, J.T., Longo, W.M., Zhang, Y., Torozo, R., Huang, Y., 2016. Identification of double-bond positions in isomeric alkenones from a lacustrine haptophyte. Rapid Commun. Mass Spectrom. 30, 112–118.

Filipova-Marinova, M., Pavlov, D., Coolen, M., Giosan, L., 2013. First high-resolution marinopalynological stratigraphy of Late Quaternary sediments from the central part of the Bulgarian Black Sea area. Quat. Int. 293, 170–183.

Giosan, L., Coolen, M.J.L., Kaplan, J.O., Constantinescu, S., Filip, F., Filipova-Marinova, M., Kettner, A.J., Thom, N., 2012. Early anthropogenic transformation of the Danube-Black Sea system. Sci. Rep. 2, 1–6.

Hay, B.J., Arthur, M.A., Dean, W.E., Neff, E.D., Honjo, S., 1991. Sediment deposition in the late Holocene abyssal Black-Sea with climatic and chronological implications. Deep-Sea Res., Part 1, Oceanogr. Res. Pap. 38, S1211–S1235.

Herrle, J.O., Bollmann, J., Gebühr, C., Schulz, H., Sheward, R.M., Giesenberg, A., 2018. Black Sea outflow response to Holocene meltwater events. Sci. Rep. 8, 1–6.

Hiscott, R.N., Aksu, A.E., 2002. Late Quaternary history of the Marmara Sea and Black Sea from high-resolution seismic and gravity-core studies. Mar. Geol. 190, 261–282.

Hiscott, R.N., Aksu, A.E., Mudie, P.J., Marret, F., Abrajano, T., Kaminski, M.A., Evans, J., Çakiroğlu, A.I., Yaşar, D., 2007. A gradual drowning of the southwestern Black Sea shelf: evidence for a progressive rather than abrupt Holocene reconnection with the eastern Mediterranean Sea through the Marmara Sea Gateway. Quat. Int. 167–168, 19–34.

Jones, G.A., Gagnon, A.R., 1994. Radiocarbon chronology of Black Sea sediments. Deep-Sea Res., Part 1, Oceanogr. Res. Pap. 41, 531–557.

Kaiser, J., Wang, K.J., Rott, D., Li, G., Zheng, Y., Amaral-Zettler, L., Arz, H.W., Huang, Y., 2019. Changes in long chain alkenone distributions and Isochrysidales groups along the Baltic Sea salinity gradient. Org. Geochem. 127, 92–103.

Konikov, E., Likhodedova, O., Pedan, G., 2007. Paleogeographic reconstructions of sea-level change and coastline migration on the northwestern Black Sea shelf over the past 18 kyr. Quat. Int. 167–168, 49–60.

Longo, W.M., Theroux, S., Giblin, A.E., Zheng, Y., James, T., Huang, Y., 2016. Temperature calibration and phylogenetically distinct distributions for freshwater alkenones: evidence from northern Alaskan lakes. Geochim. Cosmochim. Acta 180, 177–196.

M'boule, D., Chivall, D., Sinke-Schoen, D., Sinninghe Damsté, J.S., Schouten, S., van der Meer, M.T.J., 2014. Salinity dependent hydrogen isotope fractionation in alkenones produced by coastal and open ocean haptophyte algae. Geochim. Cosmochim. Acta 130, 126–135.

Major, C.O., Goldstein, S.L., Ryan, W.B.F., Lericolais, G., Piotrowski, A.M., Hajdas, I., 2006. The co-evolution of Black Sea level and composition through the last deglaciation and its paleoclimatic significance. Quat. Sci. Rev. 25, 2031–2047.

Marret, F., Mudie, P., Aksu, A., Hiscott, R.N., 2009. A Holocene dinocyst record of a two-step transformation of the Neoeuxinian brackish water lake into the Black Sea. Quat. Int. 197, 72–86.

Mertens, K.N., Bradley, L.R., Takano, Y., Mudie, P.J., Marret, F., Aksu, A.E., Hiscott, R.N., Verleye, T.J., Mousing, E.A., Smyrnova, L.L., Bagheri, S., Mansor, M., Pospelova, V., Matsuoka, K., 2012. Quantitative estimation of Holocene surface salinity variation in the Black Sea using dinoflagellate cyst process length. Quat. Sci. Rev. 39, 45–59.

Mertens, K.N., Ribeiro, S., Bouimetarhan, I., Caner, H., Combourieu Nebout, N., Dale, B., De Vernal, A., Ellegaard, M., Filipova, M., Godhe, A., Goubert, E., Grøsfjeld, K., Holzwarth, U., Kotthoff, U., Leroy, S.A.G., Londeix, L., Marret, F., Matsuoka, K., Mudie, P.J., Naudts, L., Peña-Manjarrez, J.L., Persson, A., Popescu, S.M., Pospelova, V., Sangiorgi, F., van der Meer, M.T.J., Vink, A., Zonneveld, K.A.F., Vercauteren, D., Vlassenbroeck, J., Louwye, S., 2009. Process length variation in cysts of a dinoflagellate, lingulodinium machaerophorum, in surface sediments: investigating its potential as salinity proxy. Mar. Micropaleontol. 70, 54–69.

Mudie, P.J., Rochon, A., Aksu, A.E., Gillespie, H., 2004. Late glacial, Holocene and modern dinoflagellate cyst assemblages in the Aegean-Marmara-Black Sea corridor: statistical analysis and re-interpretation of the early Holocene Noah's flood hypothesis. Rev. Palaeobot. Palynol. 128, 143–167.

Prahl, F.G., Rontani, J.F., Volkman, J.K., Sparrow, M.A., Royer, I.M., 2006. Unusual C_{35} and C_{36} alkenones in a paleoceanographic benchmark strain of Emiliania huxleyi. Geochim. Cosmochim. Acta 70, 2856–2867.

Reimer, P.J., Bard, E., Bayliss, A., Beck, J.W., Blackwell, P.G., Ramsey, C.B., Buck, C.E., Cheng, H., Edwards, R.L., Friedrich, M., Grootes, P.M., Guilderson, T.P., Haflidason, H., Hajdas, I., Hatté, C., Heaton, T.J., Hoffmann, D.L., Hogg, A.G., Hughen, K.A., Kaiser, K.F., Kromer, B., Manning, S.W., Niu, M., Reimer, R.W., Richards, D.A., Scott, E.M., Southon, J.R., Staff, R.A., Turney, C.S.M., van der Plicht, J., 2013. IntCal13 and Marine13 radiocarbon age calibration curves 0-50,000 years cal BP. Radiocarbon 55, 1869–1887.

Ross, D.A., Degens, E.T., 1974. Recent sediments of Black Sea: sediments. In: Degens, E.T., Ross, D.A. (Eds.), The Black Sea-Geology, Chemistry, and Biology. In: Memoir, vol. 20. American Association of Petroleum Geologists, pp. 183–199.

Ryan, W., Pitman, W.C., 1998. Noah's Flood: The New Scientific Discoveries About the Event That Changed History. Simon and Schuster, New York.

Ryan, W.B.F., Pitman, W.C., Major, C.O., Shimkus, K., Moskalenko, V., Jones, G.A., Dimitrov, P., Gorür, N., Sakinç, M., Yüce, H., 1997. An abrupt drowning of the Black Sea shelf. Mar. Geol. 138, 119–126.

Soulet, G., Delaygue, G., Vallet-Coulomb, C., Böttcher, M.E., Sonzogni, C., Lericolais, G., Bard, E., 2010. Glacial hydrologic conditions in the Black Sea reconstructed using geochemical pore water profiles. Earth Planet. Sci. Lett. 296, 57–66.

Soulet, G., Menot, G., Bayon, G., Rostek, F., Ponzevera, E., Toucanne, S., Lericolais, G., Bard, E., 2013. Abrupt drainage cycles of the Fennoscandian ice sheet. Proc. Natl. Acad. Sci. 110, 6682–6687.

Soulet, G., Ménot, G., Lericolais, G., Bard, E., 2011. A revised calendar age for the last reconnection of the Black Sea to the global ocean. Quat. Sci. Rev. 30, 1019–1026.

Theroux, S., D'Andrea, W.J., Toney, J.L., Amaral-Zettler, L.A., Huang, Y., 2010. Phylogenetic diversity and evolutionary relatedness of alkenone-producing haptophyte algae in lakes: implications for continental paleotemperature reconstructions. Earth Planet. Sci. Lett. 300, 311–320.

Turney, C.S.M., Brown, H., 2007. Catastrophic early Holocene sea level rise, human migration and the Neolithic transition in Europe. Quat. Sci. Rev. 26, 2036–2041.

van der Meer, M.T.J., Sangiorgi, F., Baas, M., Brinkhuis, H., Sinninghe Damsté, J.S., Schouten, S., 2008. Molecular isotopic and dinoflagellate evidence for Late Holocene freshening of the Black Sea. Earth Planet. Sci. Lett. 267, 426–434.

van Soelen, E.E., Lammers, J.M., Eglinton, T.I., Sinninghe Damsté, J.S., Reichart, G.J., 2014. Unusual C35 to C38 alkenones in mid-Holocene sediments from a restricted estuary (Charlotte Harbor, Florida). Org. Geochem. 70, 20–28.

Vidal, L., Ménot, G., Joly, C., Bruneton, H., Rostek, F., Çağatay, M.N., Major, C., Bard, E., 2010. Hydrology in the Marmara Sea during the last 23 ka: implications for timing of Black Sea connections and sapropel deposition. Paleoceanography 25. https://doi.org/10.1029/2009PA001735.

Wang, L., Longo, W.M., Dillon, J.T., Zhao, J., Zheng, Y., Moros, M., Huang, Y., 2019. An efficient approach to eliminate steryl ethers and miscellaneous esters/ketones for gas chromatographic analysis of alkenones and alkenoates. J. Chromatogr. A 1596, 175–182.

Warden, L., Moros, M., Neumann, T., Shennan, S., Timpson, A., Manning, K., Sollai, M., Wacker, L., Perner, K., Häusler, K., Leipe, T., Zillén, L., Kotilainen, A., Jansen, E., Schneider, R.R., Oeberst, R., Arz, H., Sinninghe Damsté, J.S., 2016. Climate induced human demographic and cultural change in northern Europe during the mid-Holocene. Sci. Rep. 7, 1–11.

Weiss, G.M., Massalska, B., Hennekam, R., Reichart, G.-I., Sinninghe Damsté, J.S., Schouten, S., van der Meer, M.T.J., 2020. Alkenone distributions and hydrogen isotope ratios show changes in haptophyte species and source water in the Holocene Baltic Sea. Geochem. Geophys. Geosyst. 21, e2019GC008751. https://doi.org/10.1029/2019GC008751.

Xu, L., Reddy, C.M., Farrington, J.W., Frysinger, G.S., Gaines, R.B., Johnson, C.G., Nelson, R.K., Eglinton, T.I., 2001. Identification of a novel alkenone in Black Sea sediments. Org. Geochem. 32, 633–645.

Yanchilina, A.G., Ryan, W.B.F., McManus, J.F., Dimitrov, P., Dimitrov, D., Slavova, K., Filipova-Marinova, M., 2017. Compilation of geophysical, geochronological, and geochemical evidence indicates a rapid Mediterranean-derived submergence of the Black Sea's shelf and subsequent substantial salinification in the early Holocene. Mar. Geol. 383, 14–34.

Yanchilina, A.G., Ryan, W.B.F., Kenna, T.C., McManus, J.F., 2019. Meltwater floods into the Black and Caspian Seas during Heinrich Stadial 1. Earth-Sci. Rev. 198, 102931. https://doi.org/10.1016/j.earscirev.2019.102931.

Yanko-Hombach, V., Gilbert, A.S., Dolukhanov, P., 2007. Controversy over the great flood hypotheses in the Black Sea in light of geological, paleontological, and archaeological evidence. Quat. Int. 167–168, 91–113.

Zheng, Y., Dillon, J.T., Zhang, Y., Huang, Y., 2016. Discovery of alkenones with variable methylene-interrupted double bonds: implications for the biosynthetic pathway. J. Phycol. 1050, 1037–1050.

Zheng, Y., Heng, P., Conte, M.H., Vachula, R.S., Huang, Y., 2019. Systematic chemotaxonomic profiling and novel paleotemperature indices based on alkenones and alkenoates: potential for disentangling mixed species input. Org. Geochem. 128, 26–41.

Zheng, Y., Tarozo, R., Huang, Y., 2017. Optimizing chromatographic resolution for simultaneous quantification of long chain alkenones, alkenoates and their double bond positional isomers. Org. Geochem. 111, 136–143.